


Influence of tunnel blasting construction on adjacent highway tunnel: A case study in Wuhan, China

International Journal of Protective Structures
2020, Vol. 11(3) 283–303
© The Author(s) 2019
Article reuse guidelines:
sagepub.com/journals-permissions
DOI: 10.1177/2041419619888936
journals.sagepub.com/home/prs


Zihan Liu^{1,2} , Nan Jiang¹, Jinshan Sun¹,
Yuqing Xia¹ and Guopeng Lyu¹

Abstract

In the blasting construction of new tunnels adjacent to existing tunnels, it is important to properly evaluate and control the influence of blasting vibration. In this study, the peak particle velocity of the lining structure of the Huanglongshan highway tunnel (i.e. the existing tunnel) in Wuhan, China, which was adjacent to a tunnel under construction by blasting, was monitored and analyzed. The numerical model of the existing tunnel was established by the dynamic finite element software LS-DYNA, and the reliability of the model and parameter selections were verified based on the field monitoring data. The relationship between peak particle velocity and effective tensile stress of the tunnel lining structure was proposed based on the combination of measured peak particle velocity, dynamic stress distribution characteristics, and numerical simulations under different blasting conditions. Based on the maximum tensile stress criterion and considering the dynamic tensile strength increase factor of lining material, the safety threshold of peak particle velocity for existing tunnel lining structure and the maximum charge weight for new tunnel blasting were suggested.

Keywords

Blasting vibration, adjacent existing tunnel, finite element method, field monitoring, power spectrum analysis, modal analysis

Introduction

When hard rocks are encountered during the construction of highways, railways, and subway tunnels, drilling-and-blasting method can be used. However, blasting vibration will possibly jeopardize the stability of the adjacent existing tunnel. Controlling the adverse effects of blasting vibration during new tunnel construction, proposing reasonable blasting vibration control threshold, and evaluating the safety of existing tunnel structures are the key technical problems in blasting construction adjacent to existing tunnels.

¹Faculty of Engineering, China University of Geosciences, Wuhan, China

²School of Naval Architecture, Ocean and Civil Engineering, Shanghai Jiao Tong University, Shanghai, China

Corresponding author:

Nan Jiang, Faculty of Engineering, China University of Geosciences, Wuhan 430074, China.

Email: happyjohn@foxmail.com



Figure 1. The Huanglongshan highway tunnel.

Numerous studies have investigated this topic; for example, Guo et al. (2016) used digital laser dynamic caustics experimental system and numerical simulation to study the cracking of the tunnel lining due to adjacent blasting. Some studies derived the basic influence mechanism of blasting adjacent to existing tunnels based on field monitoring and theoretical analysis (e.g. Hao et al., 2002; Chaudhary et al., 2019; Jiang and Zhou, 2012; Liang et al., 2011; Sambuelli, 2009; Xia et al., 2013). Li et al. (2013) calculated the response characteristics of shallow buried parallel adjacent tunnels according to the wave energy conservation law. With the rapid development of computer technology, many scholars began to use numerical simulation methods for related research (e.g. Li et al., 2015; Liang et al., 2013; Xu et al., 2013; Zhong et al., 2013; Zhou et al., 2017). Shin et al. (2011) used MIDAS/GTS software to establish a finite element model of existing tunnels under adjacent blasting. The simplified two-dimensional models were used in previous numerical simulation (Jiang et al., 2011; Kim et al., 2006; Lu et al., 2011; Zhu and Tang, 2006). In recent years, an increase number of studies began to use three-dimensional simulation methods for research on the influence of blasting construction on adjacent structures (Dang, 2018; Lee et al., 2016; Zhou et al., 2018). In previous studies, the new tunnel was mainly located directly above or parallel to the existing tunnel, and the parameters of the materials used in the models were based on measurements made under static conditions.

In this article, field monitoring and numerical simulations are combined to study the dynamic response characteristics of the existing tunnel under the blasting construction of the new tunnel. In this study, a new water conveyance tunnel (i.e. the new tunnel) under blasting construction is adjacent to the Huanglongshan highway tunnel (i.e. the existing tunnel). The vibration velocity of the lining structure in the existing tunnel is monitored and analyzed with the power spectral method. The simulated dynamic stress of the existing tunnel was examined, and the safety of existing tunnel was evaluated considering the material property parameters under dynamic loading condition. The results in this study can provide references for other similar projects where blasting construction method is used adjacent to existing tunnels.

Project overview

The Huanglongshan highway tunnel (existing tunnel; Figure 1) is in Wuhan, Hubei Province, China. It is a 412-m long two-way four-lane separated tunnel which was put into use in 2009. The center line of the tunnel is near north-south direction, and the center line spacing of the left

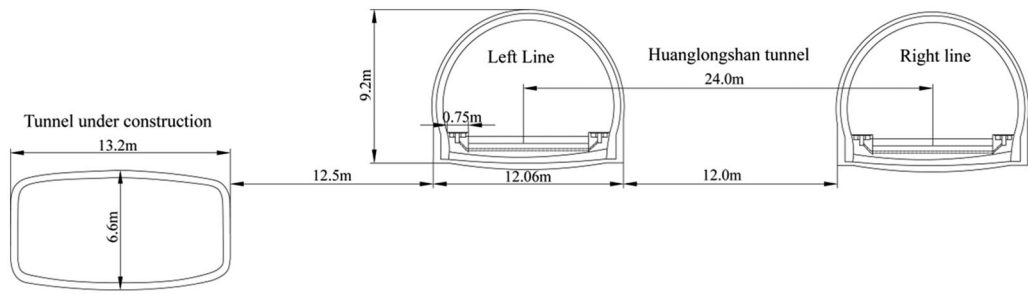


Figure 2. Relative position of new tunnel and existing tunnel.

and right line is 24 m. Along the tunnel is a denuded hill, the ground elevation is 31.0–89.6 m, the relative height difference is 58.6 m, the design elevation of the tunnel floor is 25.71–28.51 m, and the maximum cover depth is 56.15 m. The tunnel construction is based on the new Austrian tunneling method, adopting the three-center circular cross-section shape, with composite lining structure installed.

The new water conveyance tunnel starts near the north entrance of the Huanglongshan highway tunnel. The new tunnel adopts a single-box double-chamber structure with an excavation width of 13.2 m, a height of 6.6 m, a net width of 11.3 m, and a net height of 4.7 m. The new tunnel adopts the straight wall micro-arch shape cross-section.

The new tunnel was located at a lower position toward the west of the existing tunnel, and a 457.2-m long section of the new tunnel was excavated in parallel of the existing tunnel. The relative position of the new tunnel and the existing tunnel is shown in Figure 2. The horizontal clearance between the new tunnel and the existing tunnel is about 12.7 m, and the minimum distance is 12.5 m. The height difference between the new tunnel and the existing tunnel is about 8.6 m.

The new tunnel is excavated by bench excavation method. Because the horizontal clearance of the new tunnel and the left line of the existing tunnel is very small, it is the key protection section under blasting construction. The blasting vibration generated during construction will affect the existing tunnel. Taking the key protection section as the research object, the dynamic response characteristics of the lining structure in the left line of the existing tunnel have been analyzed.

Field monitoring study

Monitoring system layout

The related research shows that the influence range of blasting vibration is mainly within 20 m in front of and behind the tunnel face (Lee et al., 2016; Yao et al., 2007; Zhao et al., 2016). Therefore, a total of seven monitoring points were arranged in front of and behind the cross section of the existing tunnel closest to the new tunnel face (most unfavorable cross section), and the distance between each monitoring point was 5 m. The monitoring points were laid on the lining along the axial direction of the tunnel, as shown in Figure 3.

During the blasting construction of new tunnel, blasting vibration monitoring was carried out on the wall foot of the side facing blast of the existing tunnel, and 15 sets of reliable monitoring data were obtained. Due to limitation of the length of the paper, only representative monitoring results are taken as an example for analysis, and the most representative monitoring data are listed in Table 1. The blasting vibration monitoring uses the TC-4850 blasting vibration testing instrument and the TCS-B3 velocity sensor to measure the vibration components of the X, Y, and Z directions of the

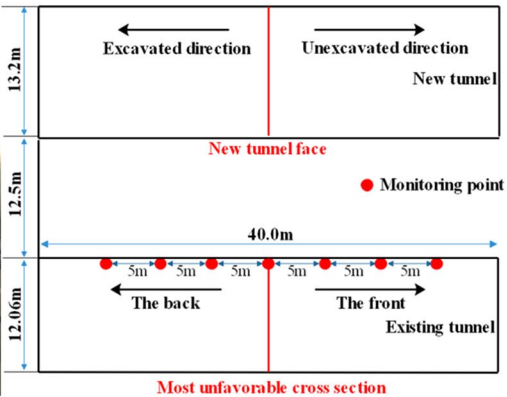


Figure 3. Arrangement of monitoring points on existing tunnel lining.

Table 1. PPV of each monitoring point.

Position	-15 m	-10 m	-5 m	0 m	+5 m	+10 m	+15 m
PPV (cm/s)							
X direction	0.382	0.773	0.816	1.414	1.06	0.998	0.820
Y direction	0.221	0.286	0.367	0.780	0.501	0.404	0.281
Z direction	0.247	0.682	0.760	0.937	0.840	0.795	0.650
Resultant velocity	0.572	1.097	1.174	1.974	1.405	1.339	1.084

PPV: peak particle velocity.

particle. The X direction is the horizontal direction perpendicular to the tunnel axis, the Y direction is perpendicular to the ground, and the Z direction is the axial direction of the existing tunnel. The 0m represents the most unfavorable cross section. The positive values represent the front of the most unfavorable cross section (i.e. the unexcavated direction of new tunnel), and the negative values represent the back of the most unfavorable cross section (i.e. the excavated direction of new tunnel).

Vibration velocity analysis of monitoring results

In order to ensure the PPV of the existing tunnel is small, the maximum charge weight per delay is controlled to 2.6kg in the construction scheme of new tunnel. This charge control scheme makes the monitoring results in Table 1 much lower than the standard value of the traffic tunnel safety PPV of 10 cm/s as stipulated in China’s Blasting Safety Regulations (AQSIQ and SAC, 2014). Therefore, from the perspective of PPV, the existing tunnel is safe.

Select the data of the monitoring point with the highest PPV to make its vibration velocity time-history curve as shown in Figure 4. In the figure, the vibration velocity curve is like a simple harmonic wave. Under the action of horizontal explosion stress wave, the PPV in the X direction is the largest in three main directions. Therefore, in the following paragraphs, the analysis of the PPV on the cross section of existing tunnel is mainly based on the PPV in the X direction.

Through the analysis of the monitoring points on the cross sections of the left line of the existing tunnel, the attenuation trend of the PPV along the axial direction of the existing tunnel is shown in Figure 5. In this figure, the 0 on the X-axis represents the most unfavorable cross section. The

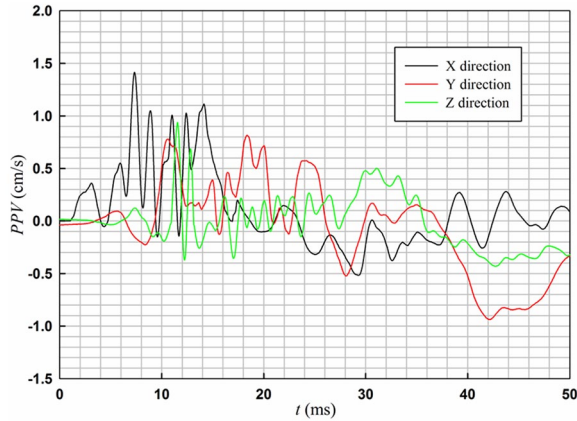


Figure 4. Vibration velocity time-history curve.

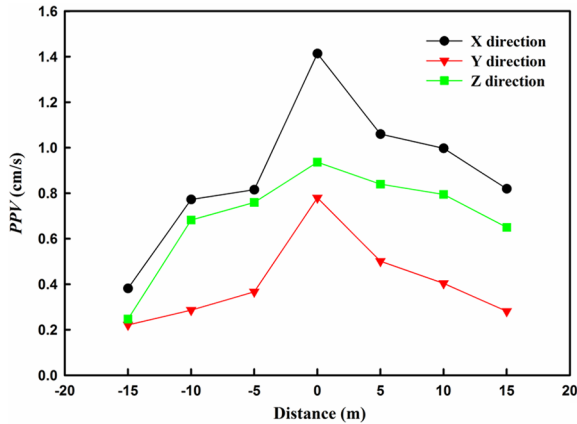


Figure 5. PPVs on each cross section of existing tunnel.

positive values represent the front of the most unfavorable cross section (i.e. the unexcavated direction of new tunnel), and the negative values represent the back of the most unfavorable cross section (i.e. the excavated direction of new tunnel).

It can be seen from Figure 5 that during the blasting construction of the new tunnel, the vibration of the most unfavorable cross section is the largest, and it tends to attenuate in front of and behind the cross section. The vibration velocity response between the front and the back of the most unfavorable cross section is quite different. The PPVs of the monitoring point in front of the cross section are greater than that of the monitoring point with the same distance behind the cross section. The attenuation of the PPV of each monitoring point in front of the cross section is slower than that of the monitoring points behind the cross section. This may be determined by the propagation law of the blasting seismic wave: the seismic wave excited by blasting propagates in the form of body wave in the rock mass. When it reaches the excavated area behind the tunnel face of new tunnel, it will form a surface wave at the interface (Person et al., 1994). When the surface wave leaves the interface, its energy will decrease exponentially with increasing distance and the surface wave will not have a great influence on the lining of adjacent existing

tunnel. The body wave can continue to propagate through the rock mass in the unexcavated area in front of the tunnel face of new tunnel, and the body wave carries a large amount of energy when propagating to the front of the cross section of the existing tunnel closest to the new tunnel face (most unfavorable cross section). There is no propagation medium behind the excavated area, so the energy of the body wave decreases and the body wave carries less energy when propagating to the back of the most unfavorable cross section. As a result, the PPVs in front of the most unfavorable cross section are greater than those of the back of the cross section, and the attenuation speed is also slow.

Spectrum analysis of monitoring results

The spectrum analysis is to transform the dynamic signal in the time domain into the frequency domain for analysis. Spectral characteristics are closely related to blasting vibration, so the spectral characteristic has become an important part of blasting vibration characteristics analysis. An important tool for spectrum analysis is the fast Fourier transform, which can identify the sine waves and their respective amplitudes of different frequency components in the blasting vibration signal (Zhao et al., 2016). The blasting vibration signal is a dynamic signal with a very complex frequency component, and one or several of these frequency components are the main frequency components. In the blasting vibration analysis, the effects of different frequency components on the structure are very different, and the power spectral density (PSD) can accurately reflect the contribution of each frequency component to the blasting vibration. Therefore, according to the fast Fourier transform, the PSD of each frequency component can better study the distribution of the main vibration frequency of the blasting vibration (Rao et al., 2017).

Defining P as the PSD of the blasting vibration signal, the formula is

$$P = \frac{|V(m)|^2}{T} \quad (1)$$

If the velocity function $V(t)$ is in the finite time domain of length T , the Fourier transform can be written as

$$V(k) = \int_0^T v(t) e^{-ikt} dt \quad (2)$$

where k is the number of waves and the data are discretized, $T = N\Delta t$ is the sampling length, and Δt is the sampling interval. When the sampling rate is 16,000, the sampling interval is 0.000625 s, which is used as the sampling standard of discrete signals for discrete Fourier transform

$$V(m) = \Delta t \sum_{n=0}^{N-1} v(n) e^{-i2\pi \frac{m}{N}} \quad 0 < m \leq N \quad (3)$$

The wave number k is discretized into $2\pi f_m$, and $f_m = m / (N\Delta t)$ is the spatial frequency. The coefficients in formula (3) ensure that the dimensions and units obtained in the PSD calculation are correct.

Substituting formula (3) into formula (1), the expression of the PSD is as following

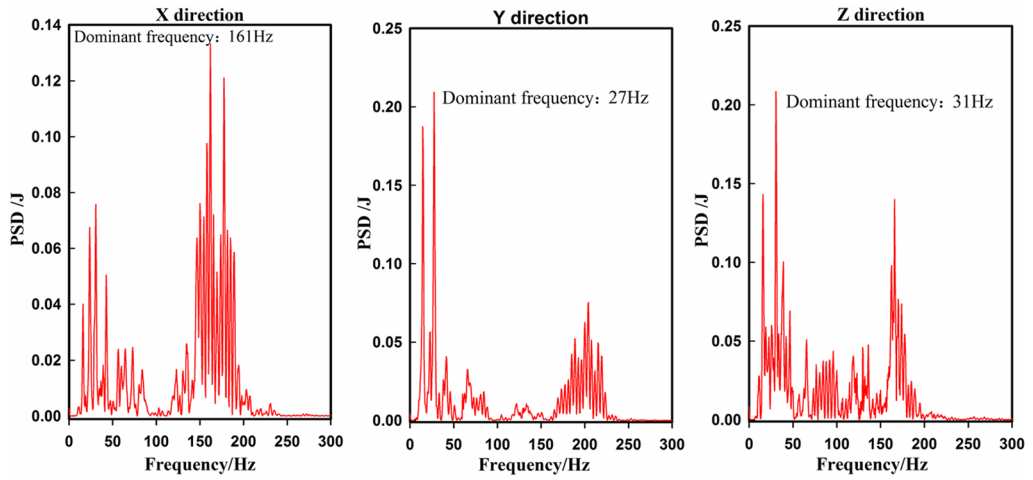


Figure 6. Power spectral density of X, Y, and Z-direction vibration signals.

$$P(m) = \frac{\Delta t}{N} \left| \sum_{n=0}^{N-1} v(n) e^{-i2\pi \frac{mn}{N}} \right|^2 \quad (4)$$

The above process is programmed by MATLAB, and the PSD curve of the blasting vibration signal is shown in Figure 6.

From the result of spectrum analysis, it can be known that the blasting vibration signal has a wide frequency band and complex frequency components. Compared with the common blasting vibration amplitude spectrum, the vibration frequency of this research is relatively large, and the vibration frequency ranged mostly from 150 to 200 Hz. The main frequency of X-direction vibration is mainly in the range of 150–190 Hz, and the main frequency is 161 Hz, but the low-frequency band 10–50 Hz also appears. The main frequency of Y-direction vibration is mainly in the range of 10–220 Hz, and the main frequency is 27 Hz, but the high-frequency band 170–220 Hz also appears. The main frequency of Z-direction vibration is mainly in the range of 10–190 Hz, and the main frequency is 31 Hz, but the high-frequency band 150–190 Hz also appears. Although the vibration response of the X direction on the tunnel lining is the most significant, from the distribution trend, the X-direction frequency is mainly concentrated in the high-frequency range of 150–190 Hz, which is much higher than the natural vibration frequency of the tunnel structure. Therefore, it will not appear resonance amplification phenomenon. The main frequency distributions of the Y and Z direction are discrete, and the distribution trends of the dominant frequencies are similar. In addition, the occurrence of low-frequency bands in the vibration signals of the two directions is more than X direction, so the resonance effect of the tunnel structure should be considered.

The dominant frequency in the power spectrum analysis is the frequency with the highest energy density in the power spectrum, but the dominant frequency displayed by the monitoring instrument is the frequency of the PPVs. It can be seen from Table 2 that the dominant frequency corresponding to the PPVs in the three directions on each monitoring point is above 100 Hz, which is much larger than the natural vibration frequency of the tunnel structure (generally below 50 Hz (Jiang et al., 2016)). Therefore, as the blasting vibration generated by the blasting construction of new

Table 2. Main frequency (Hz) corresponding to the PPV in each direction.

Position Direction	-15 m	-10 m	-5 m	0 m	+ 5 m	+ 10 m	+ 15 m
X direction	92	112	114	135	114	112	120
Y direction	156	64	2666	153	727	186	221
Z direction	102	129	94	100	666	186	103

PPV: peak particle velocity.

tunnel avoids the natural vibration frequency of the existing tunnel structure, it will not appear resonance amplification phenomenon.

Numerical simulation of the dynamic response

Numerical model

The K0+400~K0+580 section of the new tunnel is constructed by drilling-and-blasting method, which will inevitably affect the existing tunnel. This chapter selects a small section of the mileage, that is, K0+500~K0+540, as the calculation analysis area. The nonlinear dynamic finite element software ANSYS/LS-DYNA was used to analyze the influence of blasting construction of new tunnel on existing tunnel lining. The model size is 80 m × 40 m × 40 m. The X axis is a horizontal direction perpendicular to the tunnel axis, the Y axis is perpendicular to the ground, and the Z axis is the axial direction of the existing tunnel.

The method of centralized coupling charge is used to simplify the structure of the blasthole in the model, instead of multi-stage millisecond blasting in actual construction (Zhou et al., 2017, 2018). According to the relevant literature (Fang et al., 2010), the blasting vibration of the cut hole with centralized charging is the most harmful. Therefore, only the cut holes of the new tunnel face in the actual construction are selected for numerical simulation. The new tunnel face is 20 m away from the front boundary of the finite element model. The four cut-holes are divided into two rows. The hole depth is 1.1 m, the blasthole stemming length is 0.6 m, and the radius of blasthole is 2 cm (Figure 7). The four cut-holes are arranged in a wedge shape, the charging center coincides with the central axis of the new tunnel, and the total charge weight is 2.6 kg.

The whole modeling process adopts cm-g-μs unit system and Solid164 element type. The numerical model consists of 1,424,597 elements and 1,385,062 nodes. The explosion can cause large deformation with the surrounding rock and stemming. Therefore, the explosive, blasthole stemming, and surrounding rock mass elements adopt the ALE (Arbitrary Lagrange–Euler) algorithm, and the tunnel lining elements adopts the Lagrange algorithm. According to the spread of stress waves and blasting vibration monitoring data, solution time of numerical simulation in the paper was 50 ms; results of the calculation were outputted to result file every step of 0.5 μs. Figure 8 shows the finite element model, and Figure 9 shows the sectional drawing of the finite element model.

In order to reflect the contact state of various material elements realistically, rock elements and explosive elements are set to surface-to-surface sliding contact. Rock elements and concrete elements are also set to surface-to-surface contact. An automatic surface-to-surface contact mode is set between the stemming elements and the explosive elements. The surface contact algorithm is set as a surface-to-surface sliding contact between the rock elements and the stemming elements.

In order to narrow the research area and ensure the accuracy of the simulation, the rock mass with limited area is selected during modeling. For achieving energy propagation and radiation at

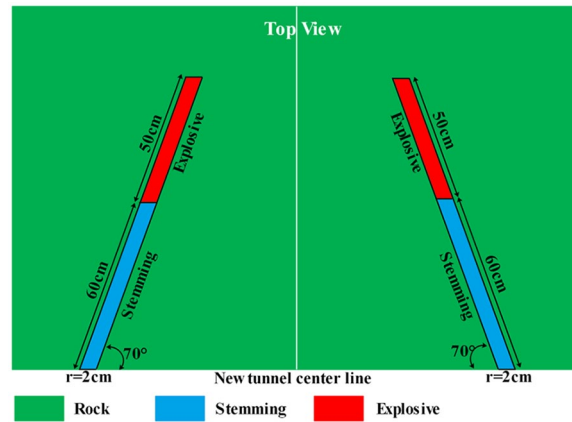


Figure 7. Top view of cut holes.

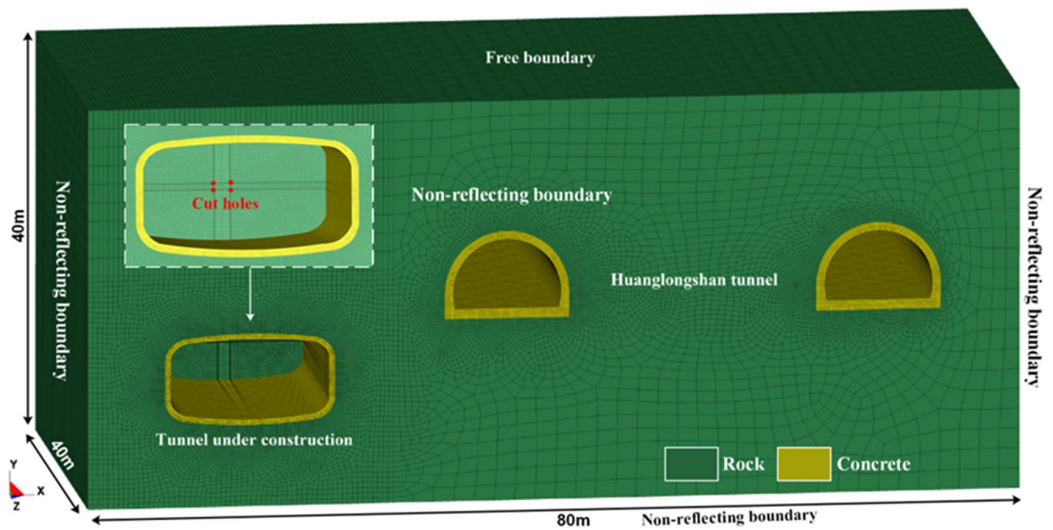


Figure 8. Finite element model.

the boundary, the left, right, front, back, and bottom boundaries of the model are set to be non-reflecting boundary to simulate the propagation of seismic waves in an infinite rock mass environment. The top of the model is set to free boundary.

Constitutive model and parameters

The explosive used in the construction of the new tunnel is 2# rock emulsion explosive. In the numerical simulation, the high-energy explosive material model MAT_HIGH_EXPLOSIVE_BURN embedded in LS-DYNA is used to simulate the detonation process of explosives. The relationship between specific volume and pressure during the explosion process is simulated by JWL (Jones–Wilkins–Lee) equation of state, and its expression is as following

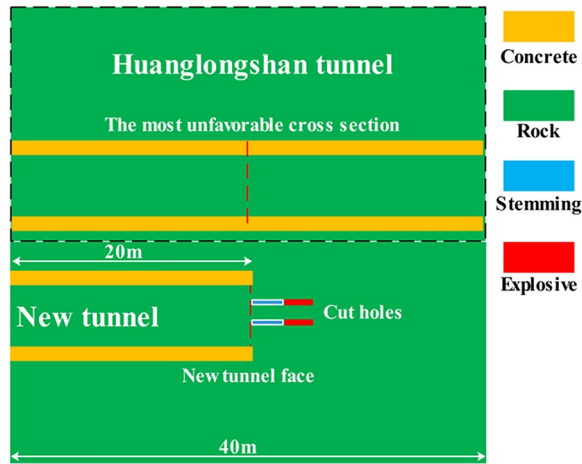


Figure 9. Sectional drawing of the finite element model.

$$p = A \left(1 - \frac{\omega}{R_1 V} \right) e^{-R_1 V} + B \left(1 - \frac{\omega}{R_2 V} \right) e^{-R_2 V} + \frac{\omega E_0}{V} \quad (5)$$

where p is the pressure; A , B , R_1 , R_2 , and ω are material constants; V is the relative volume; and E_0 is the initial specific energy. The parameters of the explosive used in the calculation are shown in Table 3.

According to the result of engineering geological survey, and combined with field test and laboratory test, the physical and mechanical parameters of rock mass and tunnel lining are obtained. The surrounding rock of the research area is limestone and classified as grade III. The constitutive model of the surrounding rock is the Drucker–Prager model, and the surrounding rock is modeled by MAT_PLASTIC_KINEMATIC material model. The material model considers the elastoplastic characteristics of rock mass. It can describe the strengthening effect and strain rate variation effect of material. This model considers the strain rate effect by introducing a strain rate factor into the yield stress according to the Cowper–Symonds model. The yield stress of the rock mass is expressed as (Hallquist, 2007)

$$\sigma_y = \left[1 + \left(\frac{\dot{\varepsilon}}{C} \right)^{\frac{1}{P}} \right] \left(\sigma_0 + \beta E_p \varepsilon_{eff}^p \right) \quad (6)$$

where σ_0 is the initial yield stress of the rock mass material, $\dot{\varepsilon}$ is the strain rate, P and C are strain rate parameters, β is an isotropic strengthening and follow-up strengthening parameter, E_p is the plastic hardening modulus, and ε_{eff}^p is the equivalent plastic strain.

According to the research conclusion of Tutuncu and Sharma (1992), the dynamic elastic modulus of rock is greater than the static elastic modulus, and the dynamic elastic modulus and static elastic modulus of limestone have the following relationship

$$E_d = 1.2196 E_s + 0.3796 \quad (7)$$

Table 3. Parameters of explosive material.

Material	Density (g/cm ³)	Detonation velocity (cm/μs)	CJ pressure (MPa)	Beta burn flag	ω	E ₀ (GPa)
Explosive	1.09	3.3	0.7	0.255	0.15	4.192

where E_d and E_s are the dynamic and static elastic modulus of limestone (GPa), respectively. Substitute the static elastic modulus of 6.0 GPa of limestone in this research, and then the dynamic elastic modulus of 7.69 GPa is obtained.

In the numerical simulation, if the reinforcement effect of the anchor on the existing tunnel lining is not considered, the calculation results can be biased toward safety. Therefore, it is assumed that the existing tunnel lining only consists of 100@0.6 steel arch centering and 20-cm thick C25 shotcrete layer. Combined with the numerical analysis experience of similar engineering, the steel arch centering in the initial support of the existing tunnel can be considered by the equivalent alternative method; that is, the elastic modulus of the steel arch centering is converted to the shotcrete layer (Hou et al., 2015; Li et al., 2014), which is calculated by the following formula

$$E = E_0 + \frac{S_g \times E_g}{S_c} \quad (8)$$

where E is the elastic modulus of concrete after conversion, E_0 is the original concrete elastic modulus with the value of 28.0 GPa (MOHURD, 2011), S_g is the cross-sectional area of the steel arch centering, E_g is the elastic modulus of the steel arch centering, and S_c is the cross-sectional area of the shotcrete layer.

The constitutive model of concrete is the Drucker–Prager model and the MAT_ELASTIC material model used. According to related literature (Liang et al., 2013; MOHURD, 2011), the dynamic elastic modulus of concrete is 30% higher than the static elastic modulus.

According to the conclusion of related research (Myung and Helander, 1972), the dynamic Poisson's ratio of the brittle materials have the following relationship, including rock mass, concrete, and the static Poisson's ratio

$$\mu_d = 2.6316\mu_s - 0.2157 \quad (9)$$

where μ_d and μ_s are dynamic and static Poisson's ratios, respectively. The static Poisson's ratio of the surrounding rock and concrete are 0.27 and 0.22, and the parameters of the surrounding rock and concrete are obtained in Table 4.

Verification of model accuracy

The numerical simulation results are compared with the monitoring results. Figure 10 shows the comparison of the X-direction vibration velocity time-history curves at the wall foot of the most unfavorable cross section. In Figure 10, the simulation results are very close to the PPV change trend of the monitoring results. The part with large vibration velocity is mainly concentrated in 0–20 ms, and the maximum vibration velocity is reached before 10 ms. After 20 ms, the vibration velocity is greatly attenuated, but there is still a residual velocity of not more than 0.5 cm/s. Although the trends of the two are roughly the same, the vibration velocity of the monitoring results changes more quickly. It may be due to the complicated geological condition in the construction area.

Table 4. Physical and mechanical parameters of materials.

Material	Density (g/cm ³)	Poisson's ratio	Shear modulus (GPa)	Elastic modulus (GPa)	Compressive strength (MPa)	Tensile strength (MPa)
Rock	2.70	0.49	3.02	7.69	46.30	0.60
Concrete	2.60	0.36	18.91	39.15	11.90	1.54
Stemming	0.85	0.35	/	1.8×10^{-4}	/	0.04

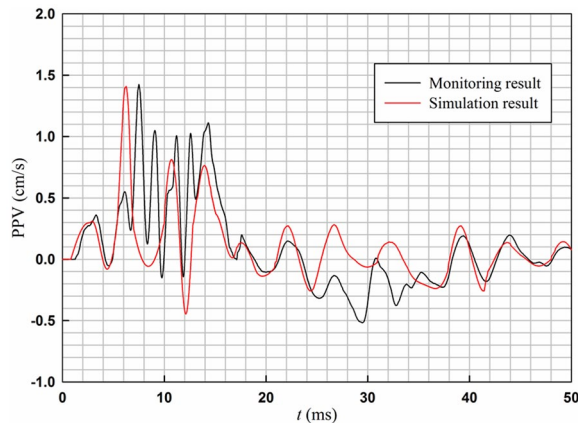


Figure 10. Comparison of monitoring results with simulation results.

Table 5 shows the comparison between the PPV of the simulation results and the monitoring results at the same position. The absolute error of the two is 0.09 cm/s, all the relative error is below 10%, and the average relative error is 7.8%. Due to the simplified processing of some construction conditions in the numerical model, such errors are acceptable in this research and the simulation result can be basically consistent with the monitoring result. The reasons why some of the monitoring results are larger than the simulation results are as following: the single-cycle excavation footage is large in some areas, so the blasthole layout is not strictly in accordance with the design scheme, or the site geological condition are not completely consistent with the result of engineering geological survey. In summary, it can be considered that the numerical calculation model reflects the actual engineering conditions well, and the analysis by numerical calculation method has high reliability and reference value.

Simulation results

Modal analysis. By modal analysis of the tunnel structure, the natural vibration frequency of the tunnel is obtained. The first 5 orders of natural vibration frequency are extracted by using the modal analysis function of the subspace iteration method in ANSYS software, which are 5.454, 10.373, 13.157, 17.433, and 21.28 rad/s. These values are much lower than the main frequency of the blasting vibration signal, so it will not appear resonance amplification phenomenon.

Vibration velocity analysis. PPV is an important indicator to evaluate the dynamic response of adjacent tunnel under blast loading. The monitoring points at the vault, arch foot, hance, wall foot, and

Table 5. Comparison of numerical simulation results and monitoring results.

Position	X-direction PPV (cm/s)			Y-direction PPV (cm/s)			Z-direction PPV (cm/s)		
	Monitoring result	Calculation result	Relative error	Monitoring result	Calculation result	Relative error	Monitoring result	Calculation result	Relative error
-15 m	0.382	0.345	9.6%	0.221	0.241	9.0%	0.247	0.232	6.1%
-10 m	0.773	0.696	9.9%	0.286	0.312	9.1%	0.682	0.613	9.9%
-5 m	0.816	0.857	5.0%	0.367	0.402	9.5%	0.760	0.714	6.0%
0 m	1.414	1.401	1.0%	0.780	0.723	7.3%	0.937	1.023	9.1%
+5 m	1.060	1.141	7.5%	0.501	0.550	9.9%	0.840	0.764	9.0%
+10 m	0.998	0.911	8.7%	0.404	0.436	7.9%	0.795	0.717	9.8%
+15 m	0.820	0.782	4.6%	0.280	0.301	7.1%	0.650	0.596	8.3%

PPV: peak particle velocity.

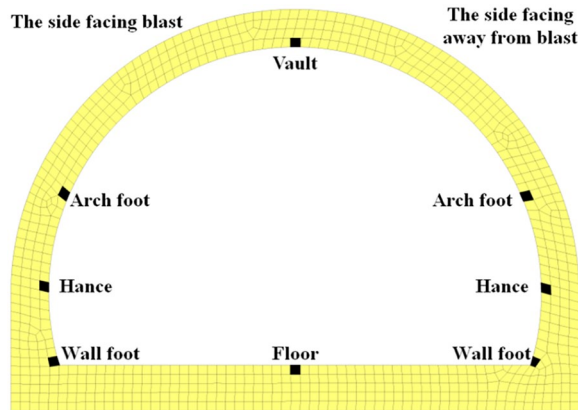


Figure 11. Distribution of monitoring points.

floor on the most unfavorable cross section are selected as the research objects, and the PPV distribution characteristics of the cross section are studied. The typical location is shown in Figure 11.

According to the conclusions of the previous paragraph, since the existing tunnel is mainly affected by the blast-induced stress wave in the horizontal direction, the X-direction PPVs at different positions are counted as shown in Figure 12. In Figure 12, the PPVs of the side facing blast is significantly larger than that of the side facing away from the blast, and the PPV of the wall foot on the side facing blast is about 10 times larger than the side facing away from the blast. Therefore, the side facing blast is the main disturbance zone under the action of blasting stress waves.

The blasting construction on the left side excites the body waves and propagates to the right side. Body waves reach the wall foot of the existing tunnel and maximize the PPV in the X direction, and then forming a surface wave by the deflection at the free surface (Person et al., 1994). In Figure 12, the X-direction PPV from the wall foot to the vault gradually decreases. The maximum PPV on the cross section is at the wall foot, followed by hance, arch foot and floor, and the PPV of the vault is the smallest. Among them, the distance between the wall foot and the explosion source is the smallest, and it is located at the geometric abrupt position. At the same time, the wall foot is affected by the collision of free surface reflection waves, so the PPV of the wall foot is the largest. The hance and the arch foot are greatly affected by the tensile stress of the reflected wave and they are relatively close to the explosion source, so the PPV of the hance and the arch foot is relatively large. The hance on the side facing away from the blast is far from the explosion source and it is isolated by the tunnel hole, and the stress wave is further attenuated, so the PPV at this position is the smallest.

The PPV at the wall foot is greater than that on other positions, reaching 1.40 cm/s, so the wall foot is a dangerous point on the cross section. The excessive PPV here may cause the tunnel lining to crack and damage, which may affect the safe operation of the existing tunnel. Therefore, in the blasting construction of the new tunnel, the monitoring and measurement on the wall foot of the existing tunnel should be strengthened.

In order to further analyze the influence of adjacent blasting on the existing tunnel, the monitoring point at the wall foot of several adjacent cross sections of the existing tunnel is selected. The PPV of each monitoring point is shown in Figure 13. In the figure, the 0 on the X-axis represents the most unfavorable cross section. The positive values represent the front of the most unfavorable cross section, and the negative values represent the back of the most unfavorable cross section.

It can be seen from Figure 13, during the blasting construction of new tunnel, the change trend of the PPVs of the axial monitoring points of the existing tunnel is large in the middle and small in the

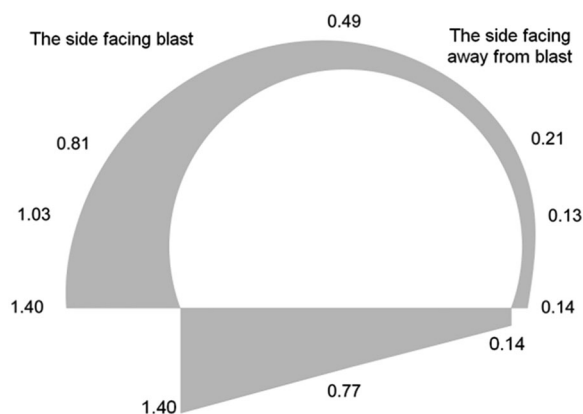


Figure 12. PPV distributions on the cross section.

two ends, which indicates that the closer the distance of the tunnel face is, the larger the PPV is. The PPV in X direction of each point is greater than that in the Y direction and that in the Z direction. As the distance from the tunnel face increases, the PPV continues to attenuate. The average attenuation index in front of the most unfavorable cross section is 1.961, and the average attenuation index behind the most unfavorable cross section is 2.065. The PPV in front of the most unfavorable cross section is generally larger than that of the particle behind the same distance from the most unfavorable cross section. The above conclusions are consistent with the field monitoring results.

Dynamic stress analysis. The above paragraphs mainly analyze the PPV, and the stress distribution is equally important for the analysis of structural stability. This section will focus on the analysis of dynamic stress of the existing tunnel lining under the adjacent blasting action. The tensile stress is positive value and the compressive stress is negative value. The dynamic stress of the typical elements (Figure 11) on the most unfavorable cross section is listed in Table 6.

It can be seen from Table 6 that the position with large stress corresponds to the position where PPV is large in the previous paragraphs. According to the elastic mechanics theory, the vibration of the surrounding rock mass causes the tunnel lining to deform in a direction, and the tensile stress of the particle in this direction is also large due to the influence of deformation coordination (Zhang et al., 2014). The dynamic stress on the side facing blast is larger than that on the side facing away from the blast. The effective tensile stress of the wall foot is relatively large, and the dynamic stress of other positions is relatively small. This is mainly because the wall foot is closer to the explosion source and is located at the geometrical abrupt change point, so the stress is greater under the influence of longitudinal wave. When the stress wave passes through the free surface, it will be converted into a surface wave, which will be diffracted when it propagates to the side facing away from the blast, causing an attenuation of energy, so the dynamic stress on the side facing away from the blast is small. Therefore, it is necessary to focus on strengthening the protection on the side facing blast of the most unfavorable cross section, and to prevent local structures from being damaged due to the dynamic response exceeding the limit. It is necessary to carry out monitoring on the wall foot. If the PPV is too large, appropriate protective measures should be taken.

In addition, since the material of tunnel lining is reinforced concrete, the material has an anti-compression ability much greater than the anti-tensile ability. Thus, the tensile stress generated under the action of the explosion stress wave is greater than the compressive stress. Therefore, the damage of the lining mainly depends on the magnitude of the tensile stress. The peak tensile stress

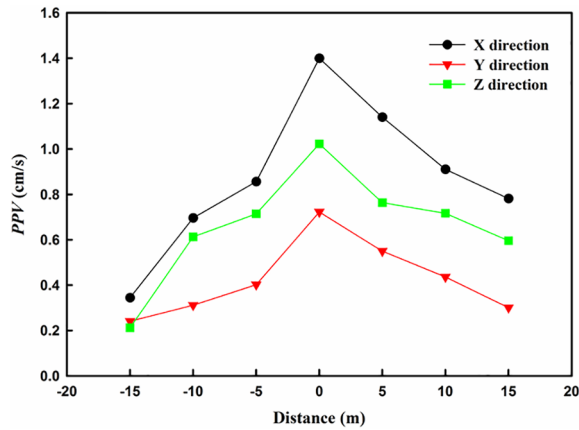


Figure 13. Comparison of PPVs of different cross sections in the axial direction.

Table 6. The stress distribution of the typical elements.

Position		Effective tensile stress (MPa)	Effective compressive stress (MPa)
The side facing blast	Wall foot	0.13	0.07
	Hance	0.07	0.06
	Arch foot	0.08	0.05
Vault		0.06	0.015
Floor		0.09	0.02
The side facing away from the blast	Wall foot	0.09	0.06
	Hance	0.027	0.026
	Arch foot	0.03	0.025

of the whole cross section is 0.13 MPa, which is less than the C25 concrete tensile strength design value of 1.27 MPa (MOHURD, 2011). The compressive stress peak value is 0.07 MPa, which is much smaller than the compressive strength design value of 11.9 MPa (MOHURD, 2011). The damage of the existing tunnel lining can be judged according to the maximum tensile stress criterion; that is, when the peak stress f_p of the lining meets the formula (10), the damage occurs

$$f_p \geq f_d \tag{10}$$

However, the peak stress on the existing tunnel lining is less than the strength design value f_d , and the strength of the structure must be greater than the design value under the dynamic load, so the tunnel is in a safe state under the blasting condition.

Since the position with the high stress in Table 6 corresponds to the position with the large PPV in the previous paragraph, there may be a functional relationship between the effective tensile stress and the PPV of the same position on the tunnel lining. Therefore, the numerical calculation of various blasting conditions was carried out by changing the charge weight and the blasting center distance. The effective tensile stress and the PPV in the X direction at the same position under different blasting conditions were analyzed and shown in Table 7. Note that China's Blasting Safety Regulations (AQSIQ and SAC, 2014) stipulate that the blasting vibration velocity threshold

Table 7. Results of numerical calculation.

Charge weight per delay (kg)	Blast center distance (m)	Effective tensile stress (MPa)	PPV (cm/s)
2.6	20.0	0.13	1.40
2.6	20.8	0.08	1.15
2.6	22.3	0.05	0.91
7.8	20.0	0.64	5.52
7.8	20.8	0.20	1.59
7.8	22.3	0.08	1.16
21.0	20.0	1.45	9.18
21.0	20.8	0.55	4.96
21.0	22.3	0.40	3.89

PPV: peak particle velocity.

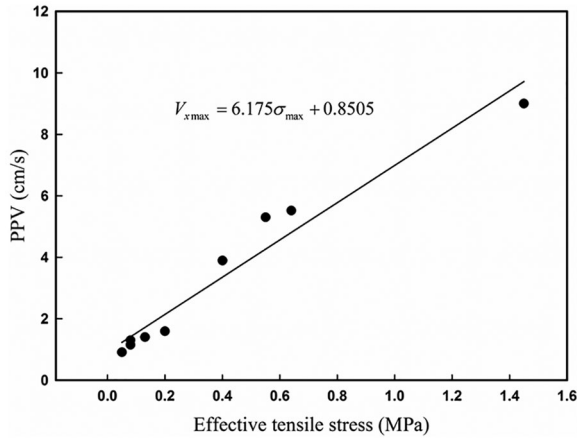


Figure 14. The statistical relationship of the effective tensile stress and X-direction PPVs.

adopts the maximum of the three components of X, Y, and Z. Therefore, in this research, the peak value of the X-direction vibration velocity is used as the research object.

Curve fitting of effective tensile stress and X-direction PPVs give the relationship as shown in Figure 14

$$V_{x\max} = 6.175\sigma_{\max} + 0.8505 \tag{11}$$

The fitting degree $R^2=0.93$, indicating that there is a strong linear relationship between the two parameters, so the PPV in the X direction can be estimated from the effective tensile stress.

Safety evaluation of existing tunnel lining

It can be seen from the previous paragraphs that the damage of the tunnel lining mainly depends on the tensile stress, so this section only discusses the tensile stress. The tensile strength of concrete under dynamic load is larger than the tensile strength under static load, and it has a correlation with strain rate (Sun et al., 2012). The European CEB-FIP model gives the calculation formula of the tensile strength dynamic increase factor (*DIF*) of concrete material (CEB, 1993)

$$DIF = \frac{f_{td}}{f_{ts}} = \begin{cases} (\dot{\epsilon}_d / \dot{\epsilon}_s)^{1.016\alpha_s} & \dot{\epsilon}_s < \dot{\epsilon} \leq 30s^{-1} \\ \gamma_s (\dot{\epsilon}_d / \dot{\epsilon}_s)^{0.33} & \dot{\epsilon} > 30s^{-1} \end{cases} \quad (12)$$

where f_{td} and f_{ts} are dynamic tensile strength and static tensile strength (MPa), respectively. $\dot{\epsilon}_d$ and $\dot{\epsilon}_s$ are dynamic strain rate and static strain rate, respectively, where $\dot{\epsilon}_s = 3 \times 10^{-6} s^{-1}$, $\gamma_s = 10^{(7.11\alpha_s - 2.33)}$, $\alpha_s = 1 / (10 + 6f_{cs} / f_{c0})$, $f_{c0} = 10$ MPa, and f_{cs} is the static compressive strength of concrete, which is 11.9 MPa.

According to the related research (Dowding, 2006), the strain of a material under blasting dynamic load is

$$\epsilon_d = \frac{v}{c} \quad (13)$$

After getting the first derivative of formula (13) with respect to time, the dynamic strain rate is

$$\dot{\epsilon}_d = \frac{\dot{v}}{c} = \frac{a}{c} \quad (14)$$

where a is the particle vibration acceleration and c is the seismic wave propagation velocity in the material, which is 3300 m/s (Guo and Fang, 1997).

After getting the first derivative of the measured vibration velocity data on the existing tunnel lining with respect to time, the particle acceleration is mostly between 10 cm/s² and 2×10^2 cm/s². According to formula (14), the dynamic strain rate on the existing tunnel lining is between 3×10^{-5} and $6 \times 10^{-4} s^{-1}$. According to formula (12), the dynamic tensile strength increase factor is between 1.22 and 1.46. Considering the most unfavorable situation, the tensile strength *DIF* is 1.22. The static tensile strength design value of C25 concrete is 1.27 MPa, multiplied by the tensile strength *DIF* of 1.22, and the dynamic tensile strength design value is 1.54 MPa. Under this condition, the tensile failure dynamic safety factor K of the tunnel lining is

$$K = \frac{f_{td}}{f_{tp}} = \frac{1.54}{0.13} = 11.9 \quad (15)$$

In the practical construction, in order to ensure the protected structure has enough safety reserves, the dynamic safety factor of the protected object is required to be above 3.0. From the calculation results, the case is in compliance with the requirements.

Substituting the dynamic tensile strength design value of concrete of 1.54 MPa into the formula (11), the corresponding allowable PPV of the lining is 10.36 cm/s, which is slightly larger than the 10 cm/s specified in China's Blasting Safety Regulations (AQSIQ and SAC, 2014). Because the design value of the dynamic tensile strength of concrete is adopted, the design value is relatively conservative and it is relatively conservative when selecting the *DIF*. Therefore, the calculated allowable PPV of 10.36 cm/s is the most conservative limit. Using this value as a warning value in blast monitoring is biased toward safety.

Based on the results of field monitoring, the empirical formula for the attenuation of the X-direction PPVs is established with reference to the Sadovskii formula (Sadovskii et al., 1966)

$$V_{x\max} = 201.89 \left(\frac{\sqrt[3]{Q}}{R} \right)^{1.422} \quad (16)$$

Substituting formula (16) into formula (11) gives the expression of the tensile stress with respect to the charge weight and the blast center distance

$$\sigma_{\max} = 32.69 \left(\frac{\sqrt[3]{Q}}{R} \right)^{1.422} - 0.8505 \quad (17)$$

The maximum tensile stress is 1.54 MPa and the blast center distance $R=20.0$ m. It can be known that the maximum allowable charge weight is 32.11 kg under this new tunnel construction, which is much larger than the current charge weight. In the subsequent construction, the charge weight can be appropriately increased to speed up the construction.

Conclusion

Both the monitoring result and the numerical simulation result show that the vibration response of the most unfavorable cross section is the largest, and it attenuates in front of and behind the cross section. There is a difference in the vibration response between the front and the back of the cross section: the PPV of the monitoring point in front of the most unfavorable cross section is greater than the PPV of the monitoring point with the same distance behind the cross section. And the attenuation of the PPVs of the monitoring points in front of the cross section is slower than that of the monitoring points behind the cross section.

Through spectrum analysis, it can be seen that the dominant frequency corresponding to the PPVs of three directions on each monitoring point is above 100 Hz, which is much larger than the natural vibration frequency of the tunnel structure obtained by modal analysis. Therefore, it will not appear resonance amplification phenomenon.

The stress response on the side facing blast is greater than that on the side facing away from the blast. The effective tensile stress of the wall foot is relatively large, reaching 0.13 MPa. The tensile stress on cross sections is generally larger than the compressive stress. The dynamic stress on the lining is less than the design value of the concrete strength, so the tunnel lining is safe. Finally, the relationship between the effective tensile stress and the X-direction PPV is established:

$$V_{x\max} = 6.175\sigma_{\max} + 0.8505.$$

The wall foot of the side facing blast of the existing tunnel should be monitored to prevent the dynamic response from being too large and causing damage. When the position of the explosion changes, the monitoring point should be set by referring to the explosion source location.

Based on the analysis of the field monitoring result and the numerical simulation result, the controlled blasting is safe to the adjacent existing tunnel and the safety factor K reaches 11.9. According to the design value of the dynamic tensile strength of concrete, the allowable PPV of the lining is 10.36 cm/s, and the maximum allowable charge weight is 32.11 kg. In the subsequent construction, the charge weight can be appropriately increased to speed up the construction.

Declaration of conflicting interests

The author(s) declared no potential conflicts of interest with respect to the research, authorship, and/or publication of this article.

Funding

The author(s) disclosed receipt of the following financial support for the research, authorship, and/or publication of this article: The authors acknowledge the financial support from the National Natural Science Foundation of China (Grant No. 41372312 and Grant No. 41807265) and the Natural Science Foundation of Hubei Province of China (Grant No. 2017CFB310).

ORCID iD

Zihan Liu  <https://orcid.org/0000-0001-7147-7218>

References

- AQSIQ and SAC (2014) *Safety Regulations for Blasting*, vol. GB6722-2014. Beijing, China: China Water Power Press.
- CEB (1993) *CEB-FIP Model Code 1990: Concrete Structures*. London: Thomas Telford.
- Chaudhary RK, Mishra S, Chakraborty T, et al. (2019) Vulnerability analysis of tunnel linings under blast loading. *International Journal of Protective Structures* 10: 73–94.
- Dang VK (2018) Impact of blasting at tunnel face on an existing adjacent tunnel. *International Journal of Geomate* 15: 22–31.
- Dowding CH (2006) Blast and construction vibration monitoring and control: thirty-five-year perspective. *Practice Periodical on Structural Design and Construction* 11: 8–12.
- Fang ZF, Li H, Yang DW, et al. (2010) Blasting parameters optimization and blasting vibration analysis of subway excavation. *Journal of Wuhan University of Technology* 32: 56–59.
- Guo D, Zhou B, Liu K, et al. (2016) Dynamic caustics test of blast load impact on neighboring different cross-section roadways. *International Journal of Mining Science and Technology* 26: 803–808.
- Guo X and Fang L (1997) Research on relation between concrete strength and stress wave velocity. *Journal of Railway Engineering Society* 54: 82–93.
- Hallquist JO (2007) *LS-DYNA Keyword User Manual (Version 971)*. Livermore, CA: Livermore Software Technology Corporation.
- Hao H, Wu C and Zhou Y (2002) Numerical analysis of blast-induced stress waves in a rock mass with anisotropic continuum damage models part 1: equivalent material property approach. *Rock Mechanics and Rock Engineering* 35: 79–94.
- Hou H, Su M, Bing Q, et al. (2015) Structural behavior of thin-walled concrete-filled steel tube used in cable tunnel: an experimental and numerical investigation. *Advances in Materials Science & Engineering* 2015: 1–12.
- Jiang L, Hu L and Lai X (2011) Investigation on the threshold control of safety blasting vibration velocity for the extraction of complicated orebody under railway. *Mining Science & Technology* 21: 169–174.
- Jiang N and Zhou C (2012) Blasting vibration safety criterion for a tunnel liner structure. *Tunnelling and Underground Space Technology* 32: 52–57.
- Jiang Y, Yang G and Wu X (2016) The nature frequency identification of tunnel lining based on the micro-tremor method. *Underground Space* 1: 108–113.
- Kim S, Jeong W, Jeong D, et al. (2006) Numerical simulation of blasting at tunnel contour hole in jointed rock mass. *Tunnelling and Underground Space Technology* 21: 306–307.
- Lee JS, Ahn SK and Sagong M (2016) Attenuation of blast vibration in tunneling using a pre-cut discontinuity. *Tunnelling and Underground Space Technology* 52: 30–37.
- Li C, Liang Q, Wu X, et al. (2014) Analysis on rigidity of primary support of composite lining and its influencing factors. *Tunnel Construction* 34: 754–759.
- Li JC, Li HB, Ma GW, et al. (2013) Assessment of underground tunnel stability to adjacent tunnel explosion. *Tunnelling and Underground Space Technology* 35: 227–234.
- Li Z, Li Q, Cui M, et al. (2015) Blasting analysis of structural vibration to highway tunnels. *Electronic Journal of Geotechnical Engineering* 3: 909–918.
- Liang Q, An Y, Lei Z, et al. (2011) Comparative study on calculation methods of blasting vibration velocity. *Rock Mechanics and Rock Engineering* 44: 93–101.

- Liang Q, Li J, Li D, et al. (2013) Effect of blast-induced vibration from new railway tunnel on existing adjacent railway tunnel in Xinjiang, China. *Rock Mechanics and Rock Engineering* 46: 19–39.
- Lu W, Yang J, Ming C, et al. (2011) An equivalent method for blasting vibration simulation. *Simulation Modelling Practice & Theory* 19: 2050–2062.
- MOHURD (2011) *Code for Design of Concrete Structures GB 50010-2010*. Beijing, China: China Architecture and Building Press.
- Myung JI and Helander DP (1972) Correlation of elastic moduli dynamically measured by in-situ and laboratory techniques. *Log Analyst* 13: 22–33.
- Person PA, Holmber R and Lee J (1994) *Rock Blasting and Explosives Engineering*. Boca Raton, FL: CRC Press.
- Rao Y, Xia Y, Yingguo HU, et al. (2017) Influence of pre-splitting crack on spectrum distribution characteristics of blasting vibration. *Journal of Vibration & Shock* 36: 191–198.
- Sadovskii MA, Adushkin VV and Rodionov VN (1966) Modeling of large ejection explosions. *Soviet Physics Doklady* 11: 1–99.
- Sambuelli L (2009) Theoretical derivation of a peak particle velocity–distance law for the prediction of vibrations from blasting. *Rock Mechanics and Rock Engineering* 42: 547–556.
- Shin J, Moon H and Chae S (2011) Effect of blast-induced vibration on existing tunnels in soft rocks. *Tunnelling and Underground Space Technology* 26: 51–61.
- Sun JS, Dou YM, Zhou J, et al. (2012) Study on effect of strain rates on the dynamic tensile properties of concrete. *Concrete* 1: 4–6.
- Tutuncu AN and Sharma MM (1992) Relating static and ultrasonic laboratory measurements to acoustic log measurements in tight gas sands. In: *SPE annual technical conference and exhibition*, Washington, DC, 4–7 October.
- Xia X, Li HB, Li JC, et al. (2013) A case study on rock damage prediction and control method for underground tunnels subjected to adjacent excavation blasting. *Tunnelling and Underground Space Technology* 35: 1–7.
- Xu PC, Dong Q, Li XP, et al. (2013) Influence research of underground caverns blasting excavation on excavation damage zone of adjacent cavern. *Advanced Materials Research* 838–841: 901–906.
- Yao Y, Chuan HE, Zhou LL, et al. (2007) Effect analysis and controlled measures research about blasting vibration to neighboring tunnel. *Journal of PLA University of Science and Technology* 8: 702–708.
- Zhang H, Gao Q, Xu B, et al. (2014) Dynamic response of tunnel lining considering both rotary and shear deformations embedded in saturated soil with seismic P wave. *Journal of Central South University (Science and Technology)* 45: 1943–1951.
- Zhao H, Long Y, Li X, et al. (2016) Experimental and numerical investigation of the effect of blast-induced vibration from adjacent tunnel on existing tunnel. *KSCE Journal of Civil Engineering* 20: 431–439.
- Zhong DW, Wu L, Yu G, et al. (2013) Study on effect of tunnelling blasting on existing adjacent tunnel. *Materials Research Innovations* 15: s513–s516.
- Zhou J, Luo Y, Li X, et al. (2017) Numerical evaluation on dynamic response of existing underlying tunnel induced by blasting excavation of a subway tunnel. *Shock and Vibration* 2017: 1–10.
- Zhou Y, Wu L, Li J, et al. (2018) The effect of blast-induced vibration on the stability of underground water-sealed gas storage caverns. *Geosystem Engineering* 21: 326–334.
- Zhu W and Tang CA (2006) Numerical simulation of Brazilian disk rock failure under static and dynamic loading. *International Journal of Rock Mechanics and Mining Sciences* 43: 236–252.